Spectrochimica Acta Part B: Atomic Spectroscopy 179 (2021) 106093

Contents lists available at ScienceDirect

Spectrochimica Acta Part B: Atomic Spectroscopy

journal homepage: www.elsevier.com/locate/sab

Analytical Note

Laser ablation molecular isotopic spectrometry for analysis of OD/OH isotopologues in plasma☆

Pengxu Ran [a,b], Genggeng Li [c], Huaming Hou [d,*]

[a] Department of Physics, Zhejiang University, Hangzhou 310027, China
[b] School of Science, Westlake University, 18 Shilongshan Road, 310024 Hangzhou, Zhejiang Province, China
[c] Key Laboratory of Advanced Technologies of Materials, Ministry of Education, Southwest Jiaotong University, Chengdu, Sichuan 610031, China
[d] Synfuels China Technology Co., Ltd., Huairou, Beijing 101407, China

ARTICLE INFO

Keywords:
Laser ablation molecular isotopic spectrometry
Laser induced breakdown spectroscopy
Molecular spectra
Heavy water

ABSTRACT

Laser ablation molecular isotopic spectrometry (LAMIS) was recently reported for isotope analysis of samples and for molecules formation mechanism investigation by analyzing the isotopologues in laser induced plasma. LAMIS was utilized to quantify the OD and OH molecules in fs-laser ablated plasma from moist water samples carried by pure Ar gas at ambient environment. A theoretical spectral fitting model for OD and OH molecules was developed and was used to extract the isotopic ratio OD/OH by fitting of experimental spectra. Time-resolved spectra were measured and the influences of spectrum intensity and signal to noise ratio (SNR) on isotopic quantitative analysis performance were evaluated. The relative concentration of OD and OH molecules in laser induced plasma from a set of water samples with D_2O concentrations in the range of 0% to 99.8% are quantified, and a very good linear relationship between D concentration and D_2O concentration was obtained. The linear curve exhibited R^2 exceeding 0.9997 and a slope of 1.006. In addition, no standard sample is necessary for quantitative analysis, demonstrating the advantages of spectral fitting LAMIS.

1. Introduction

Isotope analysis is very useful in modern scientific research areas such as energy, material and chemistry [1,2]. Analysis of isotopes is traditionally performed with mass spectrometry (MS), which involves complex sample preparation and large instrumentation, and MS is not suitable for in-situ analysis. In the past few years, optical methods has become a versatile and flexible analytical tool for quantitative isotope analysis in many research [3–5]. Laser induced breakdown spectroscopy (LIBS) is one of the frequently used optical methods for isotope analysis, in which discrete lines from neutral or ionized atoms are used. The wavelength of discrete line of isotope shifts slightly because of the mass and nuclear charge distribution difference of isotopes [6]. For LIBS, isotope analysis performance are influenced by isotope shift and peak broadening. The resolution of modern spectral detection system enables resolving discrete lines of isotopes with shifts in sub–10 pm level. However, discrete lines with small isotope shifts may not be distinguishable due to the peak broadening [4]. Therefore, LIBS based accurate quantitative isotope analysis is only applicable to elements with large isotope shifts such as hydrogen and uranium [4,7,8]. Even for hydrogen, the H_α line suffers large peak broadening and isotope analysis was mostly performed at low pressure condition to reduce the Stark broadening [9–11].

With the innovation of laser ablation molecular isotopic spectrometry (LAMIS) [5,12], the analytical performance has increased drastically and much more elements can be analyzed [13]. LAMIS takes advantage of the significant isotopic shift of molecular bands. Compared to discrete lines from neutral or ionized atoms, the isotopic shifts of molecular bands are more sensitive to the change of atom mass [5]. The isotope shifts of molecules range from tens of pm to sub-nm for molecules such as SrO, BO, CC, CN, ZrO and AlO [13–19]. LAMIS also provides a versatile tool for diagnosing formation mechanism of molecules inside plasma by isotopic labeling of some molecules. Dong et al. [20] reported LAMIS approach to elucidate the formation mechanism of C_2

☆ 'This article is published in a special honor issue dedicated to Richard E. Russo to commemorate his 70th birthday, for his achievements in the fields of laser-material interaction, plasma modeling and evolution, surface analysis with lasers, and for his vision of what is needed and critical in future theoretical, instrumental and methodological development.'

* Corresponding author.
E-mail address: Houhuaming@synfuelschina.com.cn (H. Hou).

https://doi.org/10.1016/j.sab.2021.106093
Received 17 September 2020; Received in revised form 7 December 2020; Accepted 3 January 2021
Available online 23 March 2021

and CN molecules by using ^{13}C-labeled benzonic acid. Different formation mechanisms of C_2 and CN molecules were revealed. Serrano et al. [21] investigated the formation routes of diatomic hydrogenated radicals in laser ablated plasma from deuterated molecular solids, and the result reveals that NH molecules in plasma are mainly contributed by direct release of native bonding, and hydrogenated radical may originate from diatomic carbon fragments as precursors to react with oxygen-containing species. In the work of Glaus et al. [22], LAMIS analysis is performed on laser ablated fumaric acid with a ^{13}C labeled double bond, and the results reveal that the majority of C_2 molecules originated from association of completely atomized target molecules in the early plasma, whereas in the late plasma, incomplete dissociation of carbon double bond led to the increase of C_2 molecules concentration. However, for above mentioned works, only part of molecules in the plasma were analyzed. OH molecules form in laser ablated plasma and also play a key role in tracing the chemical reaction route. Quantitative analysis of OH/OD isotopologues is still challenging because of their relatively complex molecular spectroscopic properties.

For quantitative analysis in LAMIS, there are three typically used approaches. Firstly, quantitative analysis can be performed through univariate analysis of bandhead intensity [21,22]. However, the bandheads of isotopologues typically suffer severe interference. For example, the bandheads of $^{12}C^{12}C$, ^{10}BO, $Al^{16}O$ and $^{13}C^{14}N$ suffer interference from their isotoplogues $^{13}C^{12}C$, ^{11}BO, $Al^{18}O$ and $^{12}C^{14}N$, respectively [5,17,19,20]. Moreover, (0,1) or (1,0) band is typically used for LAMIS analysis (e.g.: C_2, AlO) [13]. However, these two bands overlap with the high-J rotational lines belonging to (0,0) band [17,23]. Therefore, the intensity of bandhead hardly can be extracted by measuring the peak intensity, and the corresponding results feature poor accuracy. Secondly, isotope concentration can be predicted by chemometrics analysis, which typically offers better results than univariate analysis. However, establishing a calibration curve with a set of standard samples with known isotope concentrations is necessary, and the concentrations of isotopologues in the plasma are identical to that of corresponding isotopes is assumed. This quantitative analysis approach hardly can be used for tracking the formation routes of molecules. Thirdly, isotopologues can be quantified by fitting of experimental spectrum with synthetic spectral model of isotopologues. This methods provides a more reliable approach for LAMIS analysis because no standard sample is necessary, and the quantitative analysis results feature high accuracy and precision [13,17]. For this method, a precise spectral model is necessary. Up to now, spectral models for isotopologues such as BO, CN, C_2, AlO, ZrO and SrO have been proposed [5,13,17–19]. However, spectral models for OD and OH molecules have not been reported.

This paper describes a LAMIS method for determination of OD and OH molecules in fs-laser induced plasma. Molecular spectra of OD and OH molecules are investigated and a spectral fitting model for quantitative analysis of OD&OH molecules was proposed. Time-resolved spectra of fs-laser ablated plasma are investigated and relationships between analytical accuracy and signal-to-noise ratio (SNR) are evaluated. The method is validated by measuring a set of samples with D_2O concentration ranges from 0% to 99.8%.

2. Experimental section

2.1. Experimental setup

The experimental setup is similar to the one previously described [4]. Briefly, a Ti:Sapphire fs-laser amplifier system operated at the fundamental wavelength (centered at 800 nm) with about 35 fs pulse duration was used for ablation of gaseous water sample carried by Ar gas. The laser energy was 4 mJ/pulse and the laser beam was focused by using a plano-convex lens with f = 20 cm. The emission of plasma was coupled to the entrance slit of a 1.25 m Czerny-Turner spectrometer (Horiba, 1250 M) with imaging system containing two plano-convex lenses, and the plasma image was magnified by a factor of 2. An intensified charge coupled detector (ICCD) (Princeton instruments, MAX4, Gen III, with 2048 × 2048 pixels, 13.5 × 13.5 μm^2 per pixel, intensifier tube diameter 25 mm) was used to record the spectra. Time-resolved spectra of the emission were recorded by varying the gate delay of the ICCD with respect to the laser pulse. A grating with density of 3600 g/mm was used, which provides a spectral window of about 8 nm and resolution of 10 pm. Sample was placed in bottle and was moistened by dipping a nozzle with high purity argon gas (99.999%) passing through. The Ar gas flow was controlled by a flow meter. The moist gas passed through a 10 cm long quartz square tube, in which plasma was induced.

Pure water samples with different deuterium concentrations were prepared by mixing deuterium enriched heavy water (99.8%, ACROS) and de-ionized water. 13 samples with D_2O concentrations of 0%, 2.5%, 5%, 10%, 20%, 30%, 40%, 50%, 60%, 70%, 80%, 90% and 99.8% were prepared for measurements.

2.2. Simulation of OH/OD spectra and spectral analysis

The strongest molecular emission of OH/OD molecular band is the ultraviolet $A^2\Sigma^+ - X^2\Pi$ system. The simulation of OH/OD band spectra follows similar procedure as previous work [17], but the band structure of OH/OD is more complex compared to isotopologues such as BO, AlO, CC, CN, etc. The electronic ground state of OH/OD is an inverted $^2\Pi$ state with angular-momentum coupling intermediate between Hund's cases (a) and (b), producing two sub-levels ($F_1{}^2\Pi_{3/2}$ and $F_2{}^2\Pi_{1/2}$). The $A^2\Sigma^+$ state, which follows Hund's case (b), has two spin components (F_1 and F_2) [24]. Therefore, for each $A(v') - X(v')$ band, there are total of 12 branches, including 6 main branches (P11, Q11, R11, P22, Q22 and R22) and 6 satellite branches ($^{P}Q12$, $^{O}P12$, $^{Q}R12$, $^{Q}P21$, $^{R}Q21$ and $^{S}R21$). The intensities of the 6 main branches are much higher than those of the satellite branches. The R branch dominates the bandhead and Q branch features the highest intensity. Under thermal equilibrium condition, the rotational temperature (T_{rot}) and vibrational temperature T_{vib} are identical, and the emission intensity of a molecular band $I_{v',v'',J',J''}$ is obtained by:

$$I_{v',v'',J',J''} = C_e \frac{q_{v',v''} S_{J',J''}}{Q_{\mathrm{rot}} v'} \left(\nu_{J',J''}\right)^4 e^{-F' hc/kT_{\mathrm{rot}}} e^{-G' hc/kT_{\mathrm{vib}}} \quad (1)$$

where C_e is the emission constant, h is Plank's constant, c is the speed of light in vacuum, and k is Boltzmann constant. v and J are the vibrational and rotational quantum numbers, respectively. $q_{v',v''}$ is the Franck-Condon factors, and $S_{J',J''}$ is the Hönl-London factor. Q_{rot} is the rotational partition function. F' and G' are the rotational and vibrational energy terms of upper energy, respectively. For computing synthetic spectra, the energy levels of OD are calculated through molecular constants reported by Stark et al. [24] and the energy levels of OH are taken from Exomol database [25]. The line positions of OD and OH are directly taken from ref. [24] and ref. [25], respectively.

The simulated spectrum consists of six parameters: the relative number density of molecules (α_{OH} for OH and α_{OD} for OD), temperature (T), peak broadening ($\delta\lambda$), linear wavelength correction factor [$\beta(\lambda)$], linear intensity correction factor [$\gamma(\lambda)$]. The broadening of spectral lines is assumed to follow Lorentz profile. $\beta(\lambda)$ is used for the correction of the mismatch between the measured line positions and line positions used for spectrum calculation. $\beta(\lambda)$ is a linear function of λ with typical slope within 1±0.001. $\gamma(\lambda)$ is used for the correction of intensity deviation brought by non-identical diffraction efficiency of grating and quantum efficiency of detector over wavelength. $\gamma(\lambda)$ can be determined by calibration of the spectral detection system with standard light source. The simulation for the OH or OD band is based on the following equation:

$$I^{\mathrm{syn}}(\lambda) = \alpha \sum_i \gamma(\lambda_i) I_i(T) f\{[\beta(\lambda_i) - \lambda], \delta\lambda\} \quad (2)$$

The relative density of molecules can be calculated by fitting the experimental spectrum with simulated spectrum by locating the best

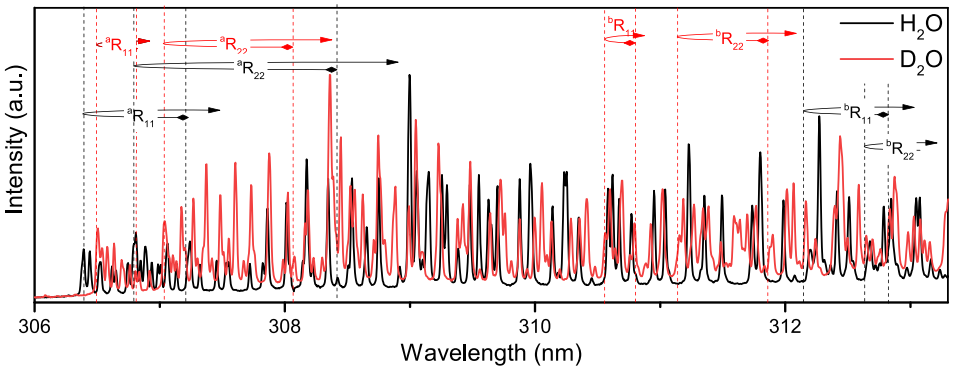

Fig. 1. Representative spectra of OH and OD from laser ablated pure H_2O and D_2O samples. ^aR and ^bR indicate (0,0, 1,1) band, respectively.

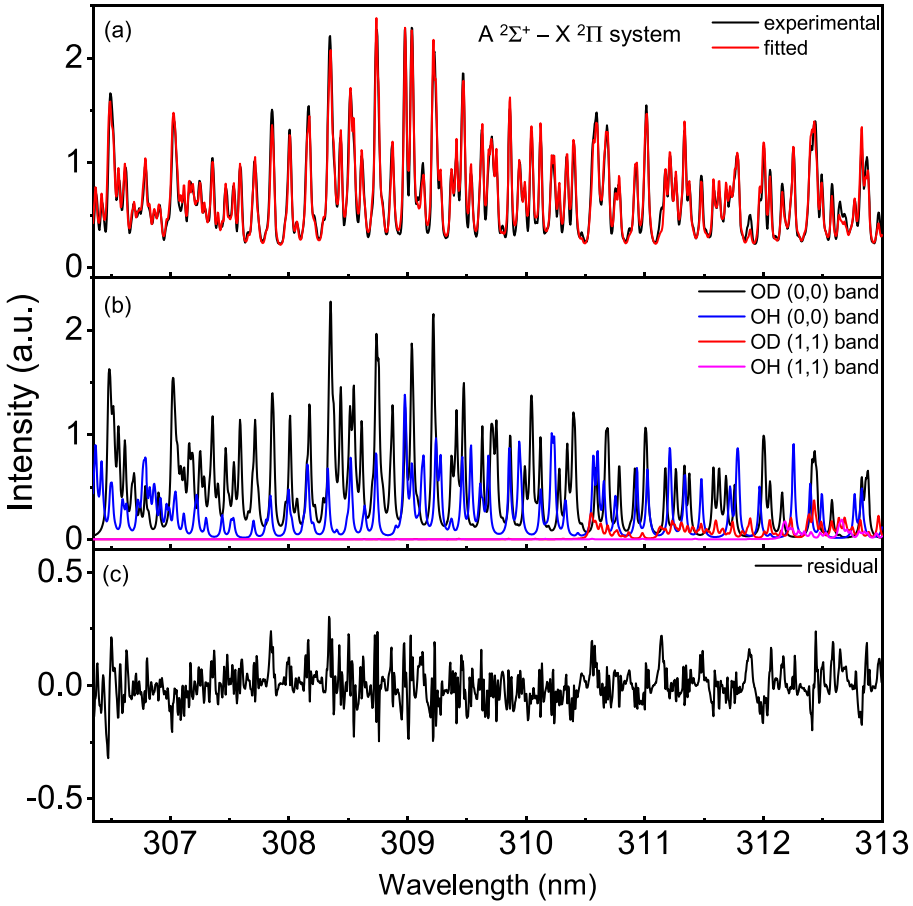

Fig. 2. Spectra fitting and band structure analysis. (a) Typical LAMIS spectrum acquired from H_2O and D_2O with identical concentration and fitted spectrum. (b) *Re*-constructed OD (0,0), OH (0,0), OD (1,1) and OH (1,1) bands through the fitting procedure. The fitting residual is shown in (c).

combination of all of the six parameters by minimization of the sum of the squares of the fitting residuals [$\varepsilon(\lambda)$] at all wavelength of the experimental spectrum, $I^{exp}(\lambda)$, through

$$I^{exp}(\lambda) = I^{syn}_{OH} + I^{syn}_{OD} + I_{continuum} + \varepsilon(\lambda) \quad (3)$$

3. Results and discussion

3.1. Analysis of molecular isotopic spectra of OH and OD

Two typical experimental spectra of laser ablated pure H_2O and D_2O samples in the range of 306 to 313.5 nm are shown in Fig. 1. The spectral range covers (0,0, 1,1) bands of $A^2\Sigma^+ - X^2\Pi$ system, and each comprises 12 branches. The bandheads of OH and OD are dominated by the R branches. The isotopic shifts of bandheads of R11 and R22 branches of (0,0) band of OD with respect to OH (Δ(OD-OH)) are 0.123 and 0.220 nm, respectively. The isotopic shifts of the Q11, Q22, P11 and P22 branches of (0,0) band are more prominent, as reported by Sarkar et al. [26] A much more prominent isotopic shifts can be observed in the (1,1) band, as seen in Fig. 1. The isotopic shift of R11 and R22 branches of (1,1) band are 1.625 and 1.602 nm, respectively. Even through the isotopic shifts of different sub-bands are quite large compared to the resolution of the spectrometer, besides R11 branch of (0,0) band, most of the bands hardly can be well distinguished due to the complex structure of OH/OD bands and severe overlap among different sub-bands.

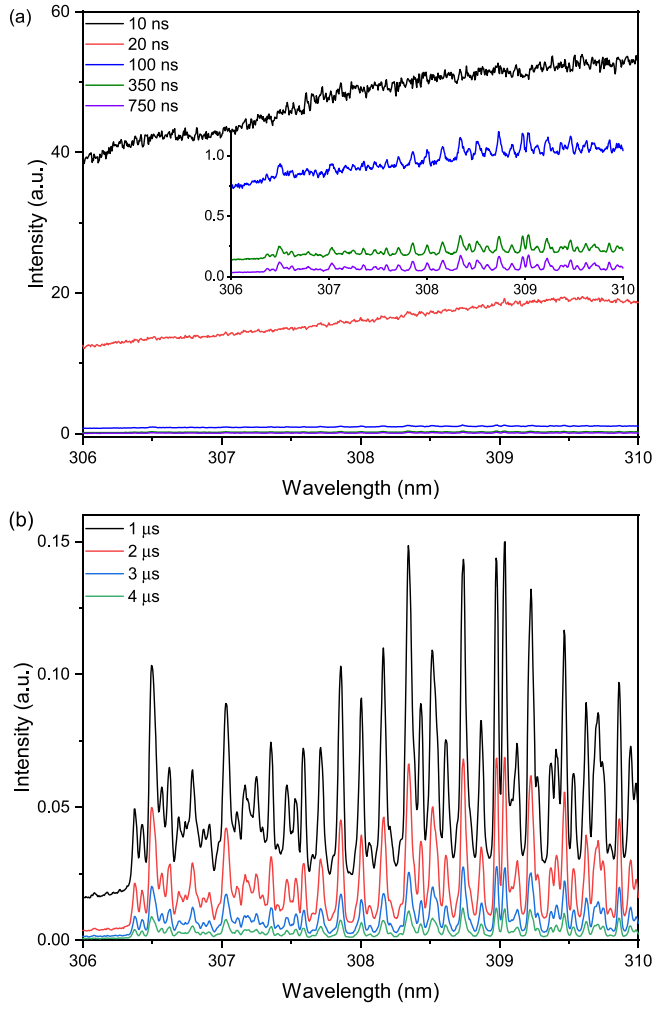

Fig. 3. Time resolved spectra from laser ablated H_2O and D_2O mixtures with identical concentration. (a) for early delay time and (b) for late delay time.

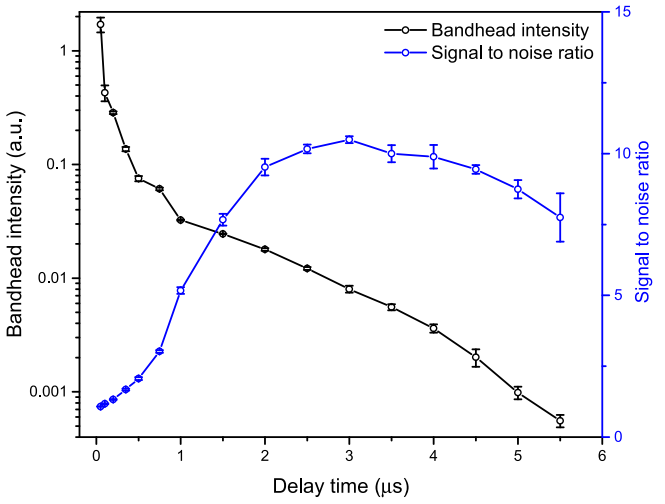

Fig. 4. Evolution of bandhead intensity of total OH and OD molecules and signal to noise ratio. Each spectrum is an integration of 1000 laser pulses.

Therefore, to perform accurate quantitative analysis, a fitting procedure is necessary to include all the contributions of different branches.

The spectral range of 306.4 to 313.0 nm was selected for spectroscopic analysis of the fs-laser induced plasma. The bandhead of R11 of (0,0) band is omitted because the quantum efficiency of the detector drops significantly in this range. A representative spectrum from laser ablated H_2O and D_2O mixtures (H_2O:D_2O=1:1) is shown in Fig. 2. Using the proposed fitting procedure, the whole spectrum can be well fitted and the band structure components of OD/OH were well reconstructed. The reconstructed band structures clearly show that the spectrum is dominated by the (0,0) band of OH and OD, and the intensity of (1,1) band is pretty weak. The reason is attributed to that the Franck-Condon factor for vibrational transition (1,1) is smaller than that of (0,0) band [27], and the vibration energy level $v = 1$ is higher than that of $v = 0$. Typical residual at each wavelength point was less than 10%, with random distribution over wavelength, indicating that the synthetic spectra model allows for quantitative analysis of OD/OH isotopologues with high accuracy.

3.2. Temporal behavior of fs-laser ablated plasma emission

The time-resolved spectra of fs-laser induced plasma emission are shown in Fig. 3. The gate widths are 50, 100, 150, 250 and 500 ns at delay times of 50, 100, 200–350, 500–750 and over 1000 ns, respectively. All the spectra are normalized to gate width and the intensities of spectra are comparable. The continuum component consisting of bremsstrahlung emission and recombination radiation from electron-ion interactions dominates the spectra acquired at delay time earlier than 20 ns, and no OH/OD fingerprint molecular spectrum was observed. The intensity of continuum spectrum drops rapidly. The molecular spectrum appears at 100 ns, and overlaps with intense continuum component. At delay time over 350 ns, the molecular spectrum becomes dominant. With further increase of delay time to 1 μs, the molecular spectrum features good SNR and persists over 4 μs. The temporal evolution of bandhead intensity and SNR are summarized in Fig. 4. The bandhead intensity represents for the peak intensity of R11 branch of (0,0) bandhead, which locates at 306.4 nm. SNR is the ratio of net bandhead intensity of R11 branch to root mean square of fluctuations of continuum background located at short wavelength side of R11 bandhead. The bandhead intensity decreases rapidly within 500 ns, and then features moderate decay until 5.5 μs. The temporal evolution of bandhead intensity shows different behavior compared to that typically observed in laser ablation of solid materials, in which case, an increasing trend of bandhead intensity was observed at early time [17] because the molecules are formed through chemical reaction between laser ablated material and air molecules. In this work, OH&OD molecules can form through direct fragmentation of water molecules. However, no molecular emission is observed at early time (Fig. 3), the reason is attributed to that the intensity of continuum spectrum is too strong, which makes the molecular emission indistinguishable.

3.3. Quantitative analysis

Quantitative analysis was performed through fitting of the experimental spectra acquired with delay time ranges from 0.75 to 3 μs. For spectra acquired earlier than delay time of 0.75 μs, the experimental spectra can not be well fitted because the spectra features low SNR. Moreover, the spectra contain intense non-flat continuum background (c.f.: Fig. 3a), which degrades the analytical performance because it is challenging to exclude the influence of non-flat continuum background through fitting procedure. For spectra acquired with delay time over 3 μs, the spectra is too weak to be fitted. Table 1 shows the comparisons of analytical bias and precision derived from spectra acquired with different delay times. The bias is the difference between predicted D_2O concentration and known D_2O concentration ($c_{predicted}$-c_{sample}). The precision is the standard deviation of three replicate measurements in absolute D_2O concentration. For the pure H_2O sample, the predicted concentrations of D_2O are about 0.3–0.7%. The predicted D_2O concentrations are typically slightly lower than the D_2O concentrations for samples with D_2O concentrations in range of 1–20%. Fitting of spectra

Table 1
Concentration of D_2O as predicted through fitting of spectra acquired at different delay times.

D_2O (%)	0.75 μs		1 μs		1.5 μs		2 μs		2.5 μs		3 μs	
	Bias (%)	Prec. (‰)	Bias (%)	Prec. (‰)	Bias (%)	Prec. (‰)	Bias (%)	Prec. (‰)	Bias (%)	Prec. (‰)	Bias (%)	Prec. (‰)
0	0.4	0.7	0.3	0.2	0.3	0.4	0.3	0.3	0.4	1.9	0.7	1.6
1	−0.1	0.9	−0.1	0.3	0.1	1.8	0.1	4.9	−0.4	2.1	−0.2	7.4
5	−0.4	0.6	−0.5	0.1	−0.4	0.2	−0.2	0.8	−1.4	2.6	−1.0	2.2
10	−0.6	0.7	−0.7	1.0	−0.7	1.3	−0.1	3.4	−1.7	3.7	−1.1	1.1
20	−0.3	0.6	−0.6	0.4	−0.7	1.0	−0.8	0.6	−0.6	3.4	−2.3	3.1
30	0.1	1.3	−0.4	0.4	−0.7	1.0	−1.1	0.1	−1.9	3.0	1.5	5.5
40	−0.5	1.4	0.4	0.3	0.6	0.1	0.5	1.1	0.5	0.5	0.3	1.5
50	−0.4	2.3	0.5	0.7	0.7	0.5	0.6	0.5	0.5	1.2	0.1	1.5
60	0.1	0.9	0.7	1.5	0.9	1.3	0.7	0.9	0.5	0.6	0.3	3.2
70	−0.8	1.7	−0.2	0.3	0.1	1.0	−0.1	1.5	−0.2	2.2	−0.6	1.0
80	−1.1	4.2	−0.5	3.0	−0.2	1.2	−0.3	1.3	−0.6	1.7	1.0	2.7
90	0.8	0.3	0.6	3.3	0.6	2.4	0.2	5.8	0.3	0.9	−0.6	2.5
99.8	0.2	0	0.2	0	0.2	0.0	0.2	0	0.2	0	0.2	0

Table 2
Comparision of prediction performance at different delay times.

Figure of merit	0.75 μs	1.0 μs	1.5 μs	2.0 μs	2.5 μs	3.0 μs
SEP	0.59%	0.49%	0.55%	0.54%	0.92%	1.00%
Slope	1.0001	1.0050	1.0060	1.0034	1.0076	0.9996
R^2	0.99979	0.99982	0.99978	0.99978	0.99936	0.99918

acquired between 0.75 and 2 μs provides a bias within ±1.2% for all samples. In some cases, the bias can be down to ±0.1%, which is comparable to most of isotopic analysis results with LAMIS [23,26,28]. With longer delay times (e.g., 2.5 and 3 μs), both bias and precision become worse, largely due to the drop of molecular band intensity. Here we note that the SNR is maximized at delay time of 2.5–3 μs (c.f.: Fig. 4), but the analytical performance degrades. The reason is attributed to that only the bandhead of (0,0) band is selected to evaluate the evolution of SNR, while both (0,0 1,1) bands are used in the fitting procedure. In addition, rotational lines constituting the bandhead of (0,0) band originate from emissions from energy levels with lower energy, and a drop of SNR of rotation lines corresponding to higher energy levels at earlier delay time is expected, especially for the rotation lines belonging to (1,1) band. Here we note that for pure D_2O sample, the predicted D_2O concentrations at all delay times are 100.0%. To access and compare the overall fitting accuracy over all sample with large D_2O concentration, standard error of prediction (SEP) was calculated for different spectra acquisition time, and the results are summarized in Table 2. Lower SEP indicates lesser error associated with prediction. Best SEP is obtained at delay time of 1 μs, and the SEP values obtained at 0.75, 1.5 and 2 μs are slightly higher. The overall prediction performance degrades at 2.5 and 3 μs. For all samples measured at delay time of 0.75–2 μs, a good linear relationship between predicted D_2O percentage and concentration of D_2O in the sample is obtained, as shown in Table 2. All the data points are well linearly fitted with R^2 exceeding 0.9997 and slopes better than 1.006. The results further demonstrate that the proposed method shows superior performance for quantitative analysis of isotopes over a wide concentration range.

For the method proposed in this work, quantitative analysis is performed by fitting the experimental spectrum with synthetic molecular isotopic spectrum, and no calibration sample set is necessary. With spectral fitting method, the relative concentration of OH/OD isotopologues in plasma plume can be predicted, which is useful for studying the chemical reactions in plasma plume. The analytical result is comparable to the results reported by Sarkar et al. [26], in which work quantitative analysis of H/D isotopes was performed with PLSR. A slightly better PLSR quantitative analysis result with SEP of 0.33% was reported by Choi et al. [29]. However, a set of standard samples is necessary for PLSR method. Moreover, quantitative analysis with PLSR methods may be limited for some applications. The spectrum from laser ablated plasma is experimental setup dependent, and the spectra of blind samples and calibration sample set should be acquired at identical conditions. Meanwhile, emission of laser ablated plasma suffers strong matrix effect [30], and a PLSR calibration matrix built with pure sample set (e.g.: mixture of H_2O and D_2O) hardly can be used for prediction of non-pure samples (e.g.: mixture of ions, H_2O and D_2O). Instead, with spectral fitting procedure, the interference spectra resulted from matrix effect can be removed by spectral deconvolution, as demonstrated in our previous works [18,31]. For the method proposed in this work, only spectrum with appropriate resolution, intensity and SNR is necessary.

4. Conclusion

Quantitative analysis of OH and OD isotopologues in fs-laser ablated plasma from water sample is reported. The isotopic shifts of the main six individual branches are analyzed and the isotopic shifts are relative large for all individual branches, especially for the branches belonging to (1,1) transitions. However, only R11 branch of (0,0) band is prominent because other branches suffering severe overlaps among different branches. Therefore, it is necessary to take the whole spectrum into account to perform quantitative analysis. A theoretical spectral model for fitting of (0,0, 1,1) band of $A^2\Sigma^+ - X^2\Pi$ system for OH and OD isotopic molecules is developed, and experimental spectrum of OH and OD can be well fitted. The temporal evolution of fs-laser ablated plasma emission is investigated and the dependence of quantitative analysis performance over intensity and SNR of spectrum are evaluated. Quantitative analysis of OD and OH molecules were performed for analysis of samples with D_2O concentrations spanning over wide range. The analytical capability is comparable with chemometric methods such as PLSR. However, the advantage of the quantitative analysis method used in this work is more prominent for measurement without standlard calibration samples. The analytical method is also very helpful for in-situ characterizing the chemical reaction routes, and for diagnosing the formation or dissociation mechanism of molecules in laser ablated plasma.

Declaration of Competing Interest

The authors declare that they have no known competing financial interests or personal relationships that could have appeared to influence the work reported in this paper.

Acknowledgement

The work is supported by National Natural Science Foundation of China (Grant No. 61605161) and Fundamental Research Funds for the

Central Universities (Grant No. 2682017CX074).

References

[1] A. Pozio, S. Tosti, Isotope effects H/D in a PEFC with PtRu/anode at low and high current density, Int. J. Hydrog. Energy 44 (14, 2019) 7544–7554, https://doi.org/10.1016/j.ijhydene.2019.01.239.

[2] R. Ogawa, H. Matsushima, M. Ueda, Hydrogen isotope separation with an alkaline membrane fuel cell, Electrochem. Commun. 70 (2016) 5–7, https://doi.org/10.1016/j.elecom.2016.06.013.

[3] S.S. Harilal, B.E. Brumfield, N.L. LaHaye, K.C. Hartig, M.C. Phillips, Optical spectroscopy of laser-produced plasmas for standoff isotopic analysis, Appl. Phys. Rev. 5 (2) (2018), 021301, https://doi.org/10.1063/1.5016053.

[4] G. Li, H. Hou, P. Ran, Y. Zhao, Z. Zhong, Calibration-free quantitative analysis of D/H isotopes with a fs-laser filament, J. Anal. At. Spectrom. 35 (2020) 1320–1329, https://doi.org/10.1039/D0JA00062K.

[5] R.E. Russo, A.A. Bol'shakov, X. Mao, C.P. McKay, D.L. Perry, O. Sorkhabi, Laser ablation molecular isotopic spectrometry, Spectrochim. Acta. Part. B. 66 (2) (2011) 99–104, https://doi.org/10.1016/j.sab.2011.01.007.

[6] J. Bauche, R.-J. Champeau, Recent progress in the theory of atomic isotope shift, in: Vol. 12 of Advances in Atomic and Molecular Physics, Academic Press, 1976, pp. 39–86, https://doi.org/10.1016/S0065-2199(08)60042-1.

[7] J. Song, G.C.-Y. Chan, X. Mao, J.D. Woodward, R.W. Smithwick, T.G. Schaaff, A. C. Stowe, C.D. Harris, R. Zheng, V. Zorba, R.E. Russo, Multivariate nonlinear spectral fitting for uranium isotopic analysis with laser-induced breakdown spectroscopy, Spectrochim. Acta. Part. B. 150 (2018) 67–76, https://doi.org/10.1016/j.sab.2018.10.008.

[8] X. Mao, G.C.-Y. Chan, I. Choi, V. Zorba, R.E. Russo, Combination of atomic lines and molecular bands for uranium optical isotopic analysis in laser induced plasma spectrometry, J. Radioanal. Nucl. Chem. 312 (2017) 121–131, https://doi.org/10.1007/s10967-017-5197-y.

[9] K.H. Kurniawan, T.J. Lie, M.M. Suliyanti, R. Hedwig, M. Pardede, D.P. Kurniawan, Y. Kusumoto, K. Kagawa, Quantitative analysis of deuterium using laser-induced plasma at low pressure of helium, Anal. Chem. 78 (16, 2006) 5768–5773, https://doi.org/10.1021/ac060633h.

[10] M. Suchoňová, P. Veis, J. Karhunen, P. Paris, M. Pribula, K. Piip, M. Laan, C. Porosnicu, C. Lungu, A. Hakola, Determination of deuterium depth profiles in fusion-relevant wall materials by nanosecond LIBS, Nucl. Mater. Energy. 12 (2017) 611–616, https://doi.org/10.1016/j.nme.2017.05.013.

[11] M. Pardede, T. Lie, J. Iqbal, M. Bilal, R. Hedwig, M. Ramli, A. Khumaeni, W. Budi, N. Idris, S. Abdulmadjid, H–D analysis employing energy transfer from metastable excited-state He in double-pulse LIBS with low-pressure He gas, Anal. Chem. 91 (2) (2018) 1571–1577, https://doi.org/10.1021/acs.analchem.8b04834.

[12] C.G. Parigger, D.M. Surmick, C.M. Helstern, G. Gautam, A.A. Bolshakov, R. E. Russo, Molecular Laser-Induced Breakdown Spectroscopy, 2020, pp. 167–209, https://doi.org/10.1016/B978-0-12-818829-3.00007-1.

[13] A.A. Bol'shakov, X. Mao, J.J. González, R.E. Russo, Laser ablation molecular isotopic spectrometry (LAMIS): current state of the art, J. Anal. At. Spectrom. 31 (2016) 119–134, https://doi.org/10.1039/C5JA00310E.

[14] X. Mao, A.A. Bol'shakov, D.L. Perry, O. Sorkhabi, R.E. Russo, Laser ablation molecular isotopic spectrometry: parameter influence on boron isotope measurements, Spectrochim. Acta. Part. B. 66 (8) (2011) 604–609, https://doi.org/10.1016/j.sab.2011.06.007.

[15] X. Mao, A.A. Bol'shakov, I. Choi, C.P. McKay, D.L. Perry, O. Sorkhabi, R.E. Russo, Laser ablation molecular isotopic spectrometry: strontium and its isotopes, Spectrochim. Acta. Part. B. 66 (11, 2011) 767–775, https://doi.org/10.1016/j.sab.2011.12.002.

[16] A. Sarkar, X. Mao, R.E. Russo, Advancing the analytical capabilities of laser ablation molecular isotopic spectrometry for boron isotopic analysis, Spectrochim. Acta. Part. B. 92 (2014) 42–50, https://doi.org/10.1016/j.sab.2013.12.001.

[17] H. Hou, X. Mao, V. Zorba, R.E. Russo, Laser ablation molecular isotopic spectrometry for molecules formation chemistry in femtosecond-laser ablated plasmas, Anal. Chem. 89 (14, 2017) 7750–7757, https://doi.org/10.1021/acs.analchem.7b01750.

[18] H. Hou, G.C.-Y. Chan, X. Mao, V. Zorba, R. Zheng, R.E. Russo, Femtosecond laser ablation molecular isotopic spectrometry for zirconium isotope analysis, Anal. Chem. 87 (9) (2015) 4788–4796, https://doi.org/10.1021/acs.analchem.5b00056.

[19] M. Dong, X. Mao, J.J. Gonzalez, J. Lu, R.E. Russo, Carbon isotope separation and molecular formation in laser-induced plasmas by laser ablation molecular isotopic spectrometry, Anal. Chem. 85 (5) (2013) 2899–2906, https://doi.org/10.1021/ac303524d.

[20] M. Dong, G.C.-Y. Chan, X. Mao, J.J. Gonzalez, J. Lu, R.E. Russo, Elucidation of C_2 and CN formation mechanisms in laser-induced plasmas through correlation analysis of carbon isotopic ratio, Spectrochim. Acta. Part. B. 100 (2014) 62–69, https://doi.org/10.1016/j.sab.2014.08.009.

[21] J. Serrano, J. Moros, J.J. Laserna, Exploring the formation routes of diatomic hydrogenated radicals using femtosecond laser-induced breakdown spectroscopy of deuterated molecular solids, J. Anal. At. Spectrom. 30 (2015) 2343–2352, https://doi.org/10.1039/C5JA00192G.

[22] R. Glaus, J. Riedel, I. Gornushkin, Insight into the formation of molecular species in laser-induced plasma of isotopically labeled organic samples, Anal. Chem. 87 (19, 2015) 10131–10137, https://doi.org/10.1021/acs.analchem.5b02926. 26402464.

[23] A. Bol'shakov, X. Mao, J. Jain, D. Mclntyre, R. Russo, Laser ablation molecular isotopic spectrometry of carbon isotopes, Spectrochim. Acta. Part. B. 113 (2015) 106–112, https://doi.org/10.1016/j.sab.2015.08.007.

[24] G. Stark, J.W. Brault, M.C. Abrams, Fourier-transform spectra of the $A^2\Sigma$–$X^2\Pi$ $\triangle v$=0 bands of OH and OD, J. Opt. Soc. Am. B. 11 (1) (1994) 3–32, https://doi.org/10.1364/JOSAB.11.000003.

[25] M. Yousefi, P.F. Bernath, J. Hodges, T. Masseron, A new line list for the $A^2\Sigma^+$–$X^2\Pi$ electronic transition of OH, J. Quant. Spectrosc. Radiat. Transf. 217 (2018) 416–424, https://doi.org/10.1016/j.jqsrt.2018.06.016.

[26] A. Sarkar, X. Mao, G.C.-Y. Chan, R.E. Russo, Laser ablation molecular isotopic spectrometry of water for $^1D_2/^1H_1$ ratio analysis, Spectrochim. Acta. Part. B. 88 (2013) 46–53, https://doi.org/10.1016/j.sab.2013.08.002.

[27] D.R. Crosley, R.K. Lengel, Relative transition probabilities and the electronic transition moment in the A–X system of OH, J. Quant. Spectrosc. Radiat. Transf. 15 (7) (1975) 579–591, https://doi.org/10.1016/0022-4073(75)90026-6.

[28] C.A. Akpovo, L. Helms, L.T. Profeta, L. Johnson, Multivariate determination of ^{10}b isotopic ratio by laser-induced breakdown spectroscopy using multiple bo molecular emissions, Spectrochim. Acta. Part. B 162 (2019), 105710, https://doi.org/10.1016/j.sab.2019.105710.

[29] S.-U. Choi, S.-C. Han, J.-I. Yun, Hydrogen isotopic analysis using molecular emission from laser-induced plasma on liquid and frozen water, Spectrochim. Acta. Part. B. 162 (2019) 105716, https://doi.org/10.1016/j.sab.2019.105716.

[30] C. Sun, Y. Tian, L. Gao, Y. Niu, T. Zhang, H. Li, Y. Zhang, Z. Yue, N. Delepine-Gilon, J. Yu, Machine learning allows calibration models to predict trace element concentration in soils with generalized LIBS spectra, Sci. Rep. 9 (2019) 11363, https://doi.org/10.1038/s41598-019-47751-y.

[31] H. Hou, G.C.-Y. Chan, X. Mao, R. Zheng, V. Zorba, R.E. Russo, Femtosecond filament-laser ablation molecular isotopic spectrometry, Spectrochim. Acta. Part. B. 113 (2015) 113–118, https://doi.org/10.1016/j.sab.2015.09.014.